REPORT DOCUMENTATION PAGE

Form approved
OMB NO. 0704-0188

Public reporting burden for this collection of information is estimated to average 1 hour per response, including the time for reviewing instructions, searching existing data sources, gathering and maintaining the data needed, and completing and reviewing the collection of information. Send comment regarding this burden estimates or any other aspect of this collection of information, including suggestions for reducing this burden, to Washington Headquarters Services, Directorate for Information Operations and Reports, 1215 Jefferson Davis Highway, Suite 1204, Arlington, VA 22202-4302, and to the Office of Management and Budget, Paperwork Reduction Project (0704-0188), Washington, DC 20503

1. AGENCY USE ONLY (*Leave blank*)	2. REPORT DATE December 2001	3. REPORT TYPE AND DATES COVCERED Final Report (4/1997—6/2001) 01 Apr 00-31 Mar 0

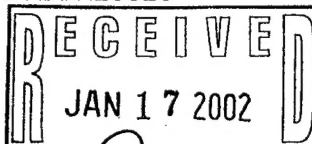| 4. TITLE AND SUBTITLE Fluid Mechanics of Compressible Dynamic Stall Control Using Dynamically Deforming Airfoils	5. FUNDING NUMBERS MIPR7ENPSAR024 MIPR8BNPSAR007 MIPR9ANPSAR005 MIPR0BNPGAR008 MIPR0KNPGAS052 ARO- MIPR
5. AUTHOR(S) M.S.Chandrasekhara	

7. PERFORMING ORGANIZATION NAME(S) AND ADDRESS(ES) Navy-NASA Joint Institute of Aeronautics, Dept. of Aeronautics & Astronautics, Code AA/CH Naval Postgraduate School, Monterey, CA 93943	8. PERFORMING ORGANIZATION REPORT NUMBER

9. SPONSORING/MONITORING AGENCY NAME(S) AND ADDRESSES U.S. Army Research Office P.O. Box 12211 Research Triangle Park, NC 27709-2211 RECEIVED JAN 17 2002 By_____	10. SPNSORING / MONITORING AGENCY REPORT NUMBER ARO-36477-EG .10

11. SUPPLEMENTARY NOTES
The views, opinions and/or findings contained in this report are those of the author(s) and should not be construed as an official Department of the Army position or decision, unless so designated by other documentation.

12a. DISTRIBUTION / AVAILABILITY STATEMENT

Approved for public release: distribution unlimited.

20020125 255

13.ABSTRACT (*Maximum 200 words*)
This report summarizes the key results from the two components of the study: (1) development of the knowledge and understanding of the fundamental fluid mechanics of the interactions of the unsteady flow occurring under the influence of the time scales of airfoil reduced frequency and dynamic leading edge adaptation at different flow conditions; (2) understanding of the role of the surface flow in compressible dynamic stall onset. For the former, a systematic investigation of the dynamic stall flow (or lack thereof) was carried out using a dynamically deforming leading edge airfoil, which allowed us to establish the fact there are some airfoil leading edge geometries that are indeed dynamic stall free. This offers the hope that rotor blade geometries can be adapted to avoid the destructive dynamic stall effects, while retaining its benefits. In the latter, 148 surface shear stress sensors were installed on an NACA 0012 airfoil and the flow behavior studied for various flow conditions, which showed the various stall onset mechanisms discovered earlier and also that the surface behavior becomes singular prior to stall onset.

14. SUBJECT TERMS Flow control, adaptive airfoils, dynamic stall, unsteady surface shear stress			15. NUMBER OF PAGES - 40 -
			16. PRICE CODE

17. SECURITY CLASSIFICATION OF REPORT UNCLASSIFIED	18. SECURITY CLASSIFICATION OF THIS PAGE UNCLASSIFIED	19. SECURITY CLASSIFICATION OF ABSTRACT UNCLASSIFIED	20. LIMITATION OF ABSTRACT UL

NSN 7540-01-280-5500   Enclosure 1   Standard Form 298 (Rev. 2-89)
Prescribed by ANSI Std. 239-1

MASTER COPY: PLEASE KEEP THIS "MEMORANDUM OF TRANSMITTAL" BLANK FOR REPRODUCTION PURPOSES. WHEN REPORTS ARE GENERATED UNDER THE ARO SPONSORSHIP, FORWARD A COMPLETED COPY OF THIS FORM WITH EACH REPORT SHIPMENT TO THE ARO. THIS WILL ASSURE PROPER IDENTIFICATION. NOT TO BE USED FOR INTERIM PROGRESS REPORTS; CLICK HERE FOR INTERIM PROGRESS REPORT INSTRUCTIONS.

MEMORANDUM OF TRANSMITTAL

U.S. Army Research Office
ATTN: AMXRO-ICA (Hall)
P.O. Box 12211
Research Triangle Park, NC 27709-2211

___ _ Reprint (Orig + 2 copies)   ___ Technical Report (Orig + 2 copies)

___ Manuscript (1 copy)   _X_ Final Progress Report (Orig + 2 copies)

__ Related materials, Abstracts, Thesis (1 copy)

CONTRACT/GRANT NUMBER: ARO-36477-EG

REPORT TITLE: Fluid Mechanics of Compressible Dynamic Stall Control Using Dynamically Deforming Airfoils

is forwarded for your information.

SUBMITTED FOR PUBLICATION TO (applicable only if report is manuscript):

_____

_____

Sincerely,

M.S.Chandrasekhara, 36477-EG

Department of Aeronautics & Astronautics

Naval Postgraduate School

Monterey, CA 93943

Enclosure 3

FLUID MECHANICS OF COMPRESSIBLE DYNAMIC STALL CONTROL USING DYNAMICALLY DEFORMING AIRFOILS

FINAL REPORT

M.S.CHANDRASEKHARA

DECEMBER 4, 2001

U.S. ARMY RESEARCH OFFICE

ARO CONTRACT NUMBER: 36477-EG

NAVY-NASA JOINT INSTITUTE OF AERONAUTICS
DEPT. OF AERONAUTICS & ASTRONAUTICS, CODE AA/CH
NAVAL POSTGRADUATE SCHOOL
MONTEREY, CA 93943

FINAL REPORT

Fluid Mechanics of Compressible Dynamic Stall Control
Using Dynamically Deforming Airfoils

FOREWORD

A three-year study was initiated to establish the fluid mechanics of compressible dynamic stall control using the concept of dynamically deforming leading edge (DDLE) airfoils in 1997. It was extended by one year to document the surface details of the airfoil compressible flow while experiencing dynamic stall. It was possible to achieve the goal of controlling dynamic stall control through flow vorticity management. Dynamically manipulating the airfoil leading edge curvature resulted in a dynamic stall free airfoil because, the consequent potential flow changes caused a redistribution of the vorticity such that it was below the critical level for coalescence. Surface hot-film gages showed that the transition moved very rapidly from the $x/c = 0.6$ towards the leading edge in a small angle of attack range, a fact crucial to computational flow modeling.

LIST OF FIGURES

Fig. 16. Development of suction peak on various airfoil configuration for M = 0.4 and k = 0.05.

Fig. 17. Attached flow envelopes for the DDLE airfoil for M = 0.3, 0.35 and 0.45.

Fig. 18. Heat flux gage outputs on the NACA 0012 airfoil upper surface, M = 0.3, k = 0.05 and upstroke.

Fig. 19. Heat flux gage outputs on the NACA 0012 airfoil upper surface, M = 0.3 and k = 0.05, upstroke, Surface map showing the rapid movement of transition point.

Fig. 20. Heat flux gage outputs on the NACA 0012 airfoil upper surface in the bubble region, M = 0.3 and k = 0.05 and upstroke.

Fig. 21. Heat flux gage outputs on the NACA 0012 airfoil upper surface showing reattachment, M = 0.3, k = 0.05 and downstroke.

Fig. 22. Heat flux gage outputs on the NACA 0012 airfoil upper surface showing shocks and shock-induced dynamic stall onset, M = 0.45 and k = 0.05.

1. STATEMENT OF THE PROBLEM STUDIED

Prior ARO funded research established that compressible dynamic stall onset mechanisms are very sensitive to leading edge flow over an airfoil and the phenomenon is dominated by the generation of a large amount of coherent vorticity near the leading edge. Thus, controlling dynamic stall requires "solutions" that can alter the leading edge flow vorticity dynamics, generally not possible given the fixed geometry of an airfoil. It is for this reason that the concept of the dynamically deforming leading edge(DDLE) airfoil was developed. The DDLE airfoil can be continuously adapted to attain the "right" shape for each instantaneous flow condition to prevent flow separation and the dynamic stall vortex from forming. It is also of interest to identify the limits of such an approach to prevent unintended consequences such as premature dynamic stall onset. Determination of the appropriate shapes for which the solution is valid requires an extensive understanding of the fundamental fluid mechanics of the interactions of the unsteady flow occurring under the influence of the time scales of airfoil reduced frequency and dynamic leading edge adaptation at different flow conditions. A major goal of the study was to develop this knowledge.

Another important flow feature of interest is the behavior of transition in this flow. The location of the transition point moves dramatically as the airfoil pitches up. Hence, it was decided to study the surface flow using densely spaced hot film gages to identify the flow events that govern the onset mechanisms. This information is also valuable in computational modeling of the flow since all flow calculations have so far assumed either fully laminar or turbulent flow, with a few exceptions that use a fixed transition location. A conventional NACA 0012 airfoil was instrumented with 148 such gages with about 60 gages located on the upper surface in the first 25% of chord (40 sensors/in) for this purpose and the flow over it was investigated.

This report summarizes the key results (drawn from the references listed in the Bibliography, Sec. 8) from these two components of the study.

Nomenclature

C_p	pressure coefficient
$C_{p_{min}}$	peak suction pressure coefficient
c	airfoil chord
f	frequency of oscillation, Hz
k	reduced frequency = $\pi f c / U_\infty$
M	freestream Mach number
p	static pressure
s, n	coordinates along and normal to airfoil surface
x,y	chordwise and vertical distance
α	angle of attack
α_o	mean angle of attack
Ω	spanwise component of vorticity

2. DESCRIPTION OF THE EXPERIMENT

2.1 The Compressible Dynamic Stall Facility

The experiments were carried out in the Compressible Dynamic Stall Facility (CDSF) located in the Fluid Mechanics Laboratory(FML) of NASA Ames Research Center. NASA and FML provided much of the instrumentation and material needed for the research. The nonintrusive optical flow measurement technique of Point Diffraction Interferometry (PDI) was used in the study. The details of the facility and the DDLE airfoil have been discussed in Ref. 1 and hence, only a very brief description is given below.

The CDSF is an in-draft wind tunnel driven by a 6MW, 240,000 CFM continuously running evacuation compressor with a 10in x 14in test section and allows for a sinusoidal variation of the airfoil angle of attack, as follows: $0 \le \alpha_m \le 15^0$, $2^0 \le \alpha_0 \le 10^0$ and $0 \le f \le$ 100Hz. A variable area downstream-throat is used to control the tunnel Mach number over the range $0.1 \le M \le 0.5$. Optical access from the stagnation point on the lower

8

surface to x/c = 0.4 on the upper surface is available with this model mounting arrangement. Flow studies over a 6-inch chord NACA 0012 supported between optical glass inserts in metal ports in the tunnel sidewalls are reported here.

2.2 The DDLE Airfoil

The philosophy used for the design of the DDLE airfoil was: relative to that of the fixed geometry airfoil,

1. reduce the suction peak pressures at high angles of attack
2. reduce the strong adverse pressure gradient
3. distribute the suction pressure over a wider region of the upper surface in order to improve the airfoil performance.
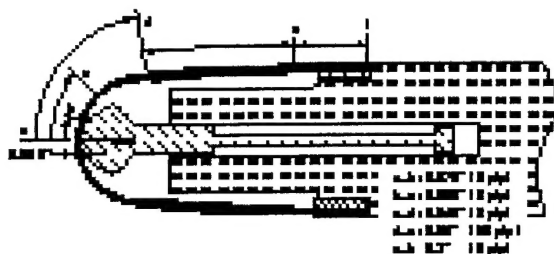
Fig. 1. Details of the DDLE airfoil model construction.
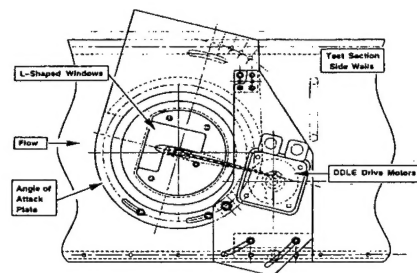
Fig. 2. Mounting arrangement of the DDLE drive system to the CDSF.

A two-piece airfoil was built, with the section $0 \leq x/c \leq 0.2$ from a carbon-fiber composite skin and the rest made from solid metal. The skin was 0.002in thick at the leading edge, but its thickness varied along its length. It was attached with a tang to a mandrel shaped to a 6-inch chord NACA 0012 leading edge profile, housed *inside* the airfoil. Fig. 1 shows model details and Fig. 2 depicts a schematic of the mounting arrangement and drive system in the CDSF. The mandrel was attached to a truss, which was in turn linked to a drive motor at each end through a connecting rod. The motors were PC controlled through software and had the capability to move the DDLE at different speeds, through a range of positions or incrementally in minimum time, to obtain a step change of shape and hold any chosen shape against the wind load and to

9

complete the required movements without jitter during movement or oscillations. Additional details of DDLE design, fabrication and control system are described in ref. 1.

2.3 The Deformation Schedule

One of the major goals of the study was to establish the hitherto unknown fluid mechanics of flow over such airfoils. With the particular design developed for this study, it was possible to vary the airfoil leading edge curvature by as much as 320% (from 0.095in radius to 0.30in radius) through a maximum leading edge retraction of 0.08in to produce dramatic flow changes around its leading edge and near the location of compressible dynamic stall onset. In this report, the various DDLE airfoil shapes used are identified by numbers, with shape 0 corresponding to that of NACA 0012. An integer shape change occurs when the airfoil chord is changed by 0.003in.
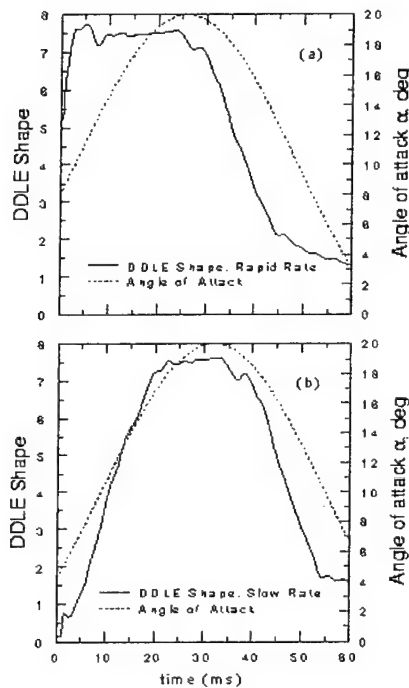
Fig. 3. DDLE airfoil shape and angle-of-attack history; $M = 0.3$, $k = 0.05$, (a) rapid adaptation and (b) slow adaptation.
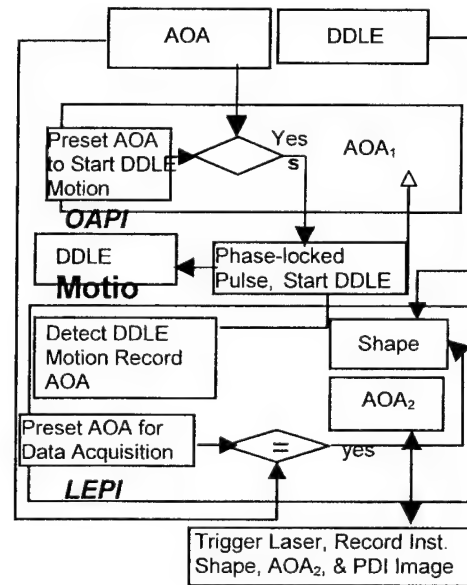
Fig. 4. Flow chart of phase-locking/data acquisition system; **LEPI**: Leading Edge Position Interface; **OAPI**: Oscillating Airfoil Position Interface.

10

A typical deformation schedule consists of rounding the nose from the original NACA 0012 shape by retracting the leading edge, holding the final shape for a dwell period, and extending the leading edge back to the original shape. Steady flow studies were used to identify stall free geometries which served as a basis to identify possible dynamic stall vortex-free geometries, based on which oscillating airfoil shape change schedules that offered the most potential for success were determined. Many different shape change schedules were used during the study. Two shape-change schedules, one fast and the other slow, along with the corresponding angle of attack variations, that were used for M = 0.3, k = 0.05 are shown in Fig. 3. The oscillations in the output response of the feedback system were minimized during the system tuning process for each condition to maintain the DDLE airfoil shape to within a half-integer of the final round shape during deformation.

2.4 Phase Locking Instrumentation

The deforming leading edge shape change is phase locked to the desired airfoil angle of attack in its sinusoidal motion cycle as shown in the flow chart in Fig. 4. Special circuitry was designed and built for this purpose. This is known as the Leading Edge Position Interface (LEPI) and works in conjunction with an existing Oscillating Airfoil Position Interface (OAPI) that was used to phase lock the airfoil angle of attack for PDI imaging. The motion was initiated by triggering the DDLE servomotor controller through a signal conditioner unit at a pre selected airfoil angle of attack. When a match occurred between the selected and actual angles of attack, the trigger pulse issued by the OAPI activated the DDLE motion controller unit, which was subsequently controlled by the pre-loaded (from the PC) software as shown in Fig. 4. A slightly varying time delay (attributable to ongoing real-time processing within the PID loop) exists in the controller leading to some uncertainty (of the order of a few encoder counts) in phase locking. Since this problem could not be eliminated, the simple solution of repeating the experiments was used satisfactorily to acquire data sets within a narrow airfoil angle of attack window of its deformation.

2.5 Instrumentation and Techniques

As stated earlier, PDI was used in the study to obtain quantitative flow field density information. Its optical arrangement was similar to that of a standard Z-type schlieren system, but the light source was a laser beam expanded (to 15 cm) to fill the field of view of interest in the test section. The optics was aligned to minimize astigmatism. The knife-edge was replaced by a pre-developed, but not fixed, (partially transmitting) photographic plate (AGFA 8E75HD). This was necessary to burn an appropriate sized pinhole in it to serve as the point diffractor and generate the reference beam. Imaging optics was set up further downstream along the beam path for recording the flow. With no flow in the test section, a pinhole was created *in situ* in the photographic plate. Light refracted by the flow density changes (signal beam) focused to a slightly different spot overlapping the point diffractor and passed through the partially transmitting photographic plate, interfering with light passing through the pin-hole (which thus becomes the reference beam) to produce interference fringes in real time, which were then recorded on Polaroid film. Ref. 2 fully describes the technique and its implementation in the CDSF.

2.6 Interferogram Image Processing

Several hundred interferograms were obtained during the experiment. These were scanned and processed manually using a software package developed in-house. Both surface and global pressure fields have been derived from the interferograms.

In these PDI images, it must be noted that increasing positive fringe numbers represent flow deceleration and vice versa. Hence, fringes from the freestream to the stagnation point have positive values, with the freestream fringe having a value of 0. The corresponding pressure along a fringe, up to the boundary layer edge, was derived using isentropic flow relations as:

$$C_p = \frac{\left[\left(\frac{\rho}{\rho_0}\right)^{\gamma} - 1\right]}{\left[\frac{\gamma}{2}M^2\right]}$$

For the specific case of the present experiments, $\rho - \rho_r = 0.009421\varepsilon$

or

$$\frac{\varrho}{\varrho_0} = \frac{\varrho_r}{\varrho_0} + 0.009421\varepsilon$$

Since ρ/ρ_0 is a function of the freestream Mach number only, ρ/ρ_0 can be determined by knowing the fringe number. The pressure at the edge of the boundary layer was then used as the surface pressure under the boundary layer assumptions.

2.7 Experimental Conditions

The experiments were conducted for a flow Mach number range from $0.2 \leq M \leq 0.45$. The corresponding Reynolds number ranged from 0.54×10^6 - 1.6×10^6. Three separate studies were completed during the study: The first one involved PDI imaging of the flow past airfoil of shapes from 0 – 22 at angles of attack of up to 20 deg, in steady flow over the above Mach number range. This was used to develop the attached flow envelope to be described later. Dynamic leading edge deformation at two rates was then used to identify the effects of the deformation time scale on the flow behavior. Based on the steady flow results, certain airfoils with fixed leading edge shapes were tested for their dynamic stall behavior when the angle of attack was varied as $\alpha = 10^0 + 10^0 \sin\omega t$. In particular, shape-2, shape-4, shape-6, shape-8, shape-8.5 and shape-10 were tested. The oscillation frequency was varied from 0 - 28 Hz, resulting in reduced frequencies from 0 - 0.1. Some shapes such as shape-8.5, shape-6, etc were found to be dynamic stall free. Since in use, a rotor has to have a sharp nose on the transonic advancing side and a rounded nose on the slower retreating side of flight, it was essential to verify the validity of the dynamic deforming leading edge approach in controlling dynamic stall when its angle of attack was also varied, with two time scales dominating the flow. These tests were also carried out. From the information generated, it was concluded that a shape change schedule from 0 – 8.5 for $M = 0.3$ and from 0 - 6 for $M = 0.4$ provided the best opportunity for controlling dynamic stall, which were then tested.

2.8 Experimental Uncertainties

The estimated uncertainties in the data are as follows:

Mach number: ± 0.005

angle of attack:	0.05 deg
reduced frequency:	0.005
airfoil shape number:	0.05
airfoil displacement:	4μm
C_p :	± 0.1
$C_{p_{min}}$:	− 5%
dCp/d(x/c) (vorticity flux):	± 25
change in α during DDLE movement:	± 0.25°

The uncertainty in C_p depends on the fringe number under consideration and is 1 fringe for the flow in general with about 3 fringes possibly undetectable near the suction peak at M = 0.3. Since correction for solid and wake blockage was less than 5% for C_p = -6.0 at M = 0.3, α = 12[0], only uncorrected PDI derived pressures are reported. The losses in the tunnel screens causing a decrease in the stagnation pressure have been included in the computation of the reference density in this otherwise atmospheric flow wind tunnel.

3. RESULTS AND DISCUSSION

3.A. Characterization of Deforming Leading Edge Airfoil Flow Regimes; M =0.3

The flow over the various airfoil shapes produced by deforming the airfoil leading edge was mapped as a function of angle of attack and leading edge shape for both fixed and dynamically changing airfoil shapes (see ref. 3). In all cases the airfoil was brought to a fixed angle of attack and held there while the leading-edge shape was varied. Each static-shape was held for several seconds before the flow was imaged. For the unsteady cases the leading edge was pulled back from shape-0 to shape-22 at different rates and the flow was conditionally sampled during the leading-edge motion by phase-locking the PDI system to one operator-selected shape per motion.

14

The results of these parametric studies are presented as flow regime maps in Fig. 5. Figure 5a shows the flow regimes that were observed for the static leading edge shapes. Shape-0, corresponding nominally to the NACA 0012 profile, first shows separation at α
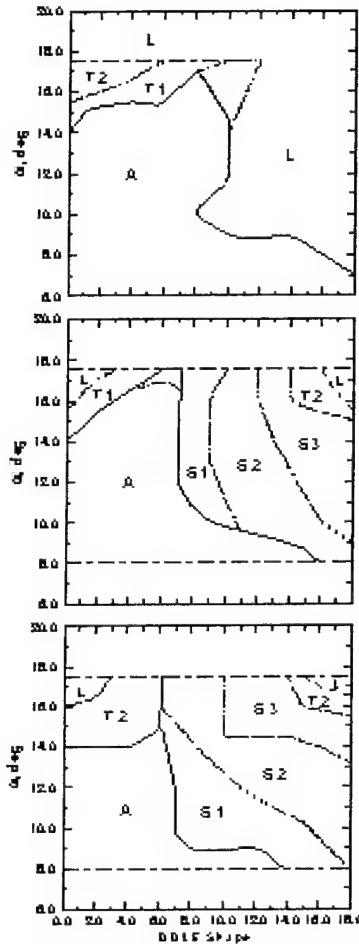
Fig. 5. Flow regimes over the DDLE airfoil: M = 0.3 and k = 0.
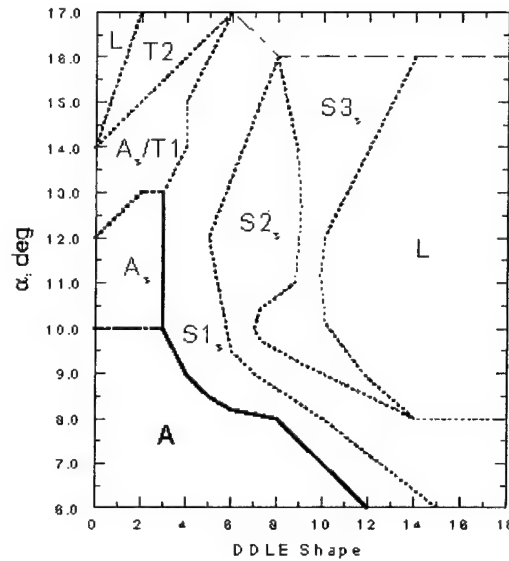
Fig. 5. Flow regimes over the DDLE airfoil: M = 0.4 and k = 0.

= 14 deg. The separation is from the trailing edge, but significant suction pressure was observed over the leading edge in the PDI image, indicating that the airfoil is producing lift (region T1 in Fig. 5a). As the angle of attack is increased, the separation progresses upstream and the leading-edge suction pressure decreases (region T2), until at 17.5deg angle of attack the flow separates from the leading edge, with a complete loss of airfoil lift (L). Note that the angle of attack at which any separation is observed increases significantly with decreasing leading-edge sharpness. This trend continues up to shape-8

for which no separation is observed until $\alpha = 17$ deg, while significant leading edge suction remains until the airfoil reaches 18 deg angle of attack. This region of leading edge suction at high angle of attack remains for shapes up to shape-12, although a high frequency vortex-shedding phenomenon appears at these higher-number shapes.

Abrupt leading-edge stall occurs at higher leading edge displacements; in fact, stall occurs at α as low as 10 deg for shape-8. It is clear form Fig. 5a that stall can be delayed up to an angle of attack of 18 degrees for a range of airfoil shapes around shape-8. It can also be seen that separated flow at high α on a sharp-nosed airfoil can be made to reattach by rounding the leading edge.

Rapidly changing the leading edge shape at a fixed angle of attack results in the development of a flow pattern very suggestive of the dynamic stall of an oscillating airfoil. This pattern can be seen in the interferograms presented in Ref. (3). The flow behavior at this deformation rate is not significantly different from that observed for fixed shapes (Fig. 5a) for shapes up to shape-6. Beyond shape-6 a fringe pattern similar to incipient dynamic stall vortex formation appears (denoted as S1 in Fig. 5b). This becomes an organized structure, which grows in size (regime S2), and moves downstream along the airfoil surface (regime S3). Only at angles of attack greater than 15 deg and for shapes rounder than shape-16 was complete leading-edge stall observed.

The flow regimes observed while changing the leading edge shape at the highest rate studied are shown in Fig. 5c. Again, as for the slow rate, a dynamic-stall-like vortex develops for shapes above shape-6. However, the fully attached flow regime is limited to angles below 14 deg; the static stall angle observed for the NACA 0012 profile. In analyzing the parts of Fig. 5, it is clear that the attached flow envelope shrinks as the rate of deformation is increased. Thus, unsteady shape change at the rates used here has caused the flow vorticity and stall behavior to be unfavorably influenced. The fact that the intermediate shapes encountered are inappropriate for the flow conditions at the angles of attack of interest is responsible for this. Since any shape adaptation involves a

rate of change of leading edge curvature, the shrinkage of the attached-flow regime suggests that a slower deformation rate is preferable at this freestream condition.

3.B. Characteristics of the DDLE Airfoil Flow at M = 0.4, Steady Flow

Figure 6 (ref. 3) shows the flow regimes as a function of static airfoil leading edge curvature and static angles of attack in steady flow at M = 0.4. Based on comparisons of interferograms (not shown) the flow over the shape-0 airfoil is similar to that over the NACA 0012 airfoil. Shocks develop in this flow at $\alpha \approx 10$deg and the airfoil experiences leading edge stall at around 14 degrees (denoted as L in Fig. 6). As the nose radius is increased at $\alpha = 6$deg, the flow remains attached until shape-12 is reached. For angles of up to 16 deg and shapes up to 4, shocks are present in the flow, but the flow does not separate; this regime is labeled A_S in Fig. 6. A fringe counting shows that the Mach number is as high as 1.2 at the foot of the shocks. Eventually, the shocks induce a small-scale separation above 12 deg for shape-4 and beyond ($S1_S$). Even with the shocks present over the upper surface, the flow remains in that state until angles of attack of about 17 deg when leading edge stall occurs. This stall angle is much higher than the 12 deg stall angle observed for the NACA 0012, showing the considerable alleviation of separation that can be obtained by rounding the leading edge.

The small-scale separation grows progressively more severe for rounder leading edge shapes (regimes $S2_S$ and $S3_S$), and eventually complete separation from the leading edge is observed.

3.C. Flow Details Over Shape-8.5 Airfoil; M = 0.3, k = 0.05

As discussed for Fig. 5a, there exists a range of airfoil shapes in flow at M = 0.3 in which flow separation is delayed up to $\alpha = 18$deg, for the steady conditions. Thus, it was decided to investigate the behavior of an oscillating airfoil with a fixed nose shape within this range as the next step in assessing the effectiveness of the DDLE airfoil concept for achieving dynamic stall control. Several airfoils having leading edge shapes similar to shape-8 were tested while executing sinusoidal pitching oscillations. In the tests, the DDLE leading edge curvature was held fixed at a predetermined value. Flow images over

the shape-8.5 airfoil will be presented below since this shape provided the maximum delay of unsteady separation, while noting that the flow over shapes-7.5 and 8 were qualitatively similar.

The PDI image (ref. 3) in Fig. 7a for α = 11.02deg indicates that the flow is attached everywhere because the fringes turn smoothly around the airfoil nose and return gradually towards the surface and the boundary layer fringes run nearly parallel to the surface; a pattern observed in prior tests during attached flow conditions. Since the fringes represent constant density lines and the flow is attached, the image also presents global and surface pressure information. A similar flow pattern is present even at α = 17.02deg, Fig. 7b (note that there is some separation downstream of the leading edge, but the flow near the leading edge is attached). For comparison, deep dynamic stall was found to occur (Ref. 4) by α = 16deg over an oscillating NACA 0012 airfoil at these same flow conditions, with a corresponding loss in leading-edge suction, whereas in the present case, the flow near the leading edge is still attached at 17 deg. At α = 19.01deg (Fig. 7c), a larger region of separated flow can be seen towards the rear of the airfoil, but even at this high angle of attack, the leading edge flow is fully attached. The separation seen in the image is trailing edge flow reversal moving upstream. Figure 7d shows that the leading edge flow is attached also at α = 20.0deg; this is a major improvement of the flow behavior. An even more important result is the absence of the dynamic stall vortex in the separated flow region in complete contrast to what is normally seen on oscillating airfoils. Thus, for the DDLE shape-8.5 airfoil it has been possible to maintain a vortex-free flow at all angles of attack during oscillation. This is a significant result because the strong and detrimental pitching moment variations concomitant with a convecting vortex have now been eliminated on this single element airfoil, even at high angles of attack.

The attached leading edge flow allows the airfoil to continuously produce lift throughout the upstroke. During the downstroke, the flow reattaches towards the trailing edge, Fig. 7e α = 15.49deg) and 7f (α = 13.97deg). As the airfoil develops less lift at the lower angles of attack, the leading edge vorticity must be shed, which seems to happen through the occurrence of light dynamic stall over a small angle of attack range, based on analysis

of the interferograms. In Fig. 7f, the fringe pattern seen near the leading edge confirms this, as the airfoil flow adapts to this lower angle of attack. In summary, although the airfoil experienced stall, it is a much softer stall wherein the flow over the leading edge remains attached and the vorticity developed at high angles of attack is shed through mild trailing edge stall.

3.D. PDI Images of Shape-6 Airfoil Flow; M = 0.4, k = 0.05

Although the shape-8.5 airfoil displayed excellent flow characteristics at M = 0.3 and k = 0.05, dynamic stall, with a well-defined dynamic stall vortex, occurred on this shape at M = 0.4 and k = 0.05 (not shown). Since shape-8.5 was on the border of the envelope of attached flow with shocks in steady flow at M = 0.4, a sharper leading edge shape-6 was studied for M = 0.4. These tests showed that the DDLE shape 6 airfoil behaved in a manner similar to the shape-8.5 airfoil at M = 0.3 and k = 0.05. Representative
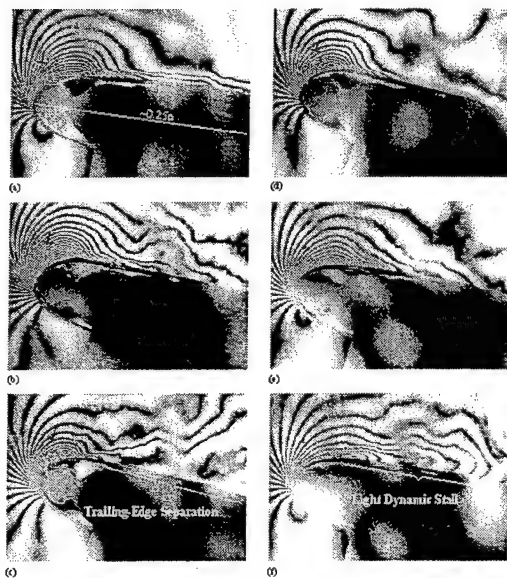
Fig. 7. PDI Images of the DDLE shape 8.5 airfoil; M = 0.3 and k = 0.05; (a) α = 11.02 deg; (b) α = 17.02 deg; (c) α = 19.01 deg; (d) α = 20 deg; (e) α = 15.09 deg $\downarrow$; (f) α = 13.97 deg$\downarrow$.
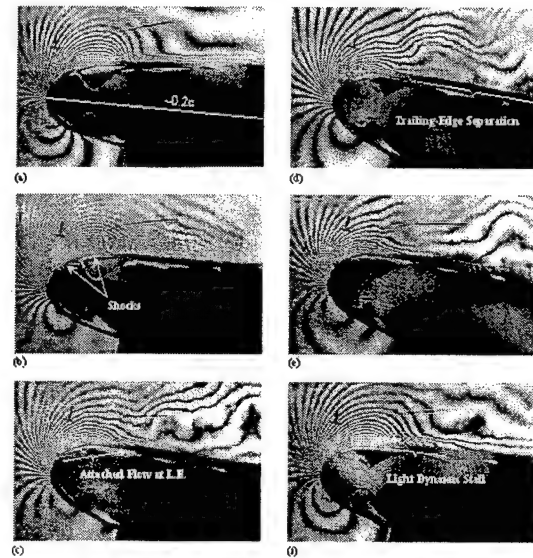
Fig. 8. PDI Images of the DDLE shape 6 airfoil; M = 0.M and k = 0.05; (a) α = 7.97 deg; (b) α = 12.03 deg; (c) α = 18.0 deg; (d) α = 20 deg; (e) α = 18.0 deg $\downarrow$; (f) α = 13.97 deg$\downarrow$.

interferograms for this flow are presented in Fig. 8 a-f (ref. 3). At an angle of attack of 7.97 deg, Fig. 8a shows that the flow is fully attached, with a $C_{P_{min}}$ of -2.92. The

interferograms showed a fringe pattern with two peaks by $\alpha = 10$deg (not shown). The critical $C_{P_{min}}$ of -3.66 was also exceeded by this angle and shocks appeared at higher angles. Figure 8b shows the multiple shocks which formed at $\alpha = 11.98$ deg. Some flow disturbances can be seen at the foot of the last shock in the figure; however, the fringes indicate attached flow. This flow pattern continued until $\alpha = 16$deg, when trailing edge separation was seen (not shown). Figure 8c shows for $\alpha = 18$deg that the leading edge flow is still attached, although with fewer fringes, and shows some trailing edge separation beyond $x/c \approx 0.3$. The decrease in the number fringes represents a corresponding decrease in the local peak suction value, which is about -3.24 for this case. It is believed that the increased wake width due to trailing edge separation has altered the airfoil pressure distribution, and has caused the leading edge flow to become subsonic again. Figure 8d for $\alpha = 20$deg shows that the trailing edge separation has progressed to $x/c \approx 0.15$, yet the leading edge flow remains attached at the top of the upstroke. During the downstroke, the separated portion of the flow reattaches progressively toward the trailing edge. Attached flow can be seen up to $x/c \approx 0.25$ in Fig. 8e for $\alpha = 18$deg. At an angle of attack of 13.97 deg, Fig. 8f, the flow appears to have fully reattached, but the fringes near $x/c \approx 0.1$-0.15 show an incipient vortex, like the light dynamic stall seen for the shape 8.5 airfoil at $M = 0.3$ and $k = 0.05$ (Fig. 8f). It seems that shape-6 provides the conditions to prevent the formation of a deep dynamic stall vortex and the corresponding strong pitching moment variations. The formation of shocks in the flow implies that the stall onset mechanisms for these conditions are significantly different from those at $M = 0.3$. That the DDLE airfoil did not experience abrupt dynamic stall even at this Mach number confirms the applicability of the concept for a variety of flow conditions.

3.E. Airfoil Pressure and Vorticity Flux Distributions; $M = 0.3$, $k = 0.05$

As described by Reynolds and Carr [5], when no transpiration is present, the vorticity flux in a flow with a moving surface is given in simplified form by

$$\nu \frac{\partial \Omega}{\partial n} = \frac{\partial U_s}{\partial t} + \frac{1}{\varrho} \frac{\partial p}{\partial s}$$

An order or magnitude analysis (ref. 3) shows that the surface acceleration term in the above equation is about 2 orders smaller and hence can be neglected initially. Thus, one can obtain the vorticity fluxes from the pressure distributions by simply taking the derivative with respect to distance along the airfoil surface.
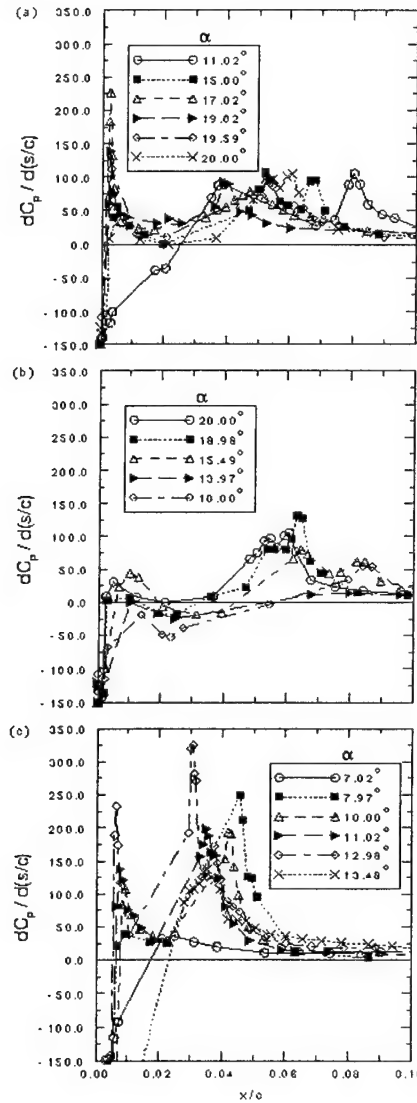

Fig. 9. Vorticity flux distributions; M = 0.3 and k = 0.05. (a) DDLE shape 8.5 airfoil, upstroke; (b) DDLE shape 8.5 airfoil, downstroke; and (c) NACA 0012 airfoil.

The vorticity fluxes calculated from the pressure distributions are plotted in Fig. 9a and 9b for the shape-8.5 airfoil and Fig. 9c for the NACA 0012 airfoil. The distributions

in Fig. 9a for the airfoil upstroke show that generally there are two peaks in vorticity flux for the higher angles shown; a larger amplitude narrow one at the suction peak location and a smaller amplitude, wider one further downstream. For smaller angles the two peaks are away from the leading edge region. The larger peaks shown have about twice the amplitude of the smaller peaks, but the latter are several times wider. Since the area under the curve gives the total vorticity production, the broader distributions provide a greater contribution to this term. As the angle of attack increases, the second peak moves progressively closer to the leading edge; for example it is at $x/c = 0.08$ for $\alpha = 11.02$deg and at $x/c = 0.04$ for $\alpha = 19$deg. As the airfoil reaches the top of the cycle, there is a reduction in the peak vorticity flux that is produced because the degree of unsteadiness decreases to zero. Also, the data indicate a movement of the vorticity flux peaks toward the trailing edge for $\alpha = 19.59$deg and $\alpha = 20$deg. The maximum value indicated in the graph is about 230 for the first peak for $\alpha = 17$deg, but generally the value for most distributions in the second peak is around 100-125. The decrease in the first peak for $\alpha \geq$ 17deg may be attributable to the trailing edge separation that was discussed in Sec. C.

During the airfoil downstroke the peak values drop as the angle of attack is decreased and the peak also moves towards the trailing edge. It should be noted that the vorticity has to decrease due to the decreasing angle of attack and the excess vorticity has to be shed in order for the ☐flow to adjust to the rapidly changing conditions ☐In Fig. 9c the distribution of vorticity flux for the NACA 0012 airfoil peaks with a magnitude of around 250. At a low angle of attack of 8deg this peak is centered near $x/c = 0.04$, but it moves close to the leading edge and is around $x/c = 0.025$ for 13deg with a magnitude of about 350. The PDI images for the NACA 0012 airfoil show that dynamic stall ensued at $\alpha =$ 14deg for this ☐case. Also, no trailing edge separation could be identified in the PDI images of the NACA 0012 ☐for this case; the trailing-edge separation appears to provide a mechanism for shedding the vorticity at the high angles at which the DDLE airfoil was tested. It is believed that for the vorticity to coalesce into a vortex, these sharp high peak values are necessary. The vortex thus formed has to be convected by the flow. Eventually, flow separation follows, causing unacceptably large hysteresis in the load and moment loops. By carefully lowering the peak levels, and distributing the total vorticity

22

over a greater area on the airfoil upper surface, it becomes possible to keep the flow attached and produce lift at low drag values until higher angles of attack.

3.F. Characteristics of the DDLE Airfoil Flow at M = 0.3, k = 0.05

In this section, the results for the case of the dynamically deforming leading edge airfoil will be discussed. Whereas the previous two sections have shown the superior performance of certain fixed shape airfoils, the need for a DDLE airfoil arises in the helicopter case because the rotor blade has to fly through a large speed range. The transonic advancing side requires a sharper nose compared to the lower speed retreating side. Thus, dynamic adaptation becomes necessary. As a consequence, two time scales
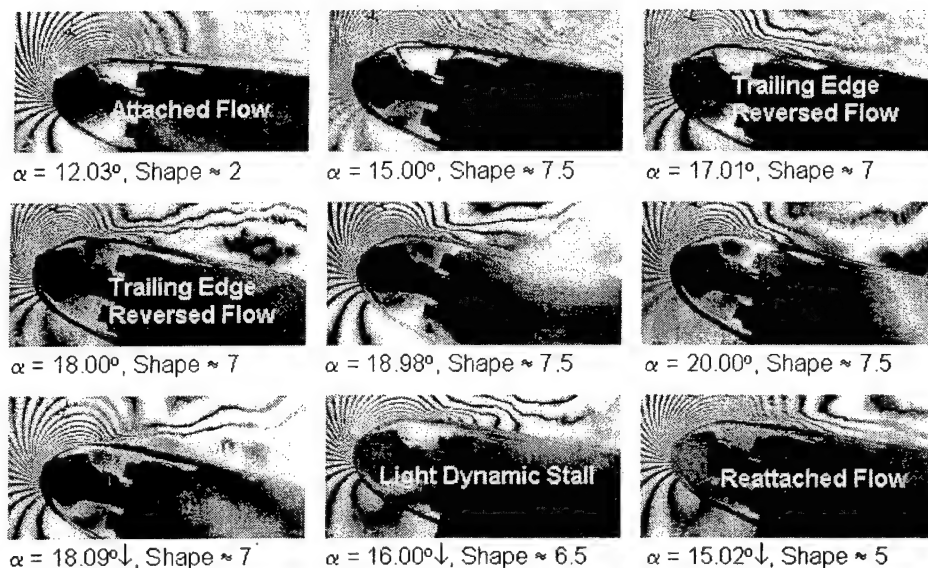
Fig. 10. PDI Images of flow over the SAP airfoil; M = 0.3, k = 0.05 and rapid adaptation

enter the flow physics and it becomes important to identify if this causes any fundamental flow changes.

The PDI images of the flow at M = 0.3 and k = 0.05 over the DDLE airfoil adapted from shape-0 (NACA 0012) to shape-8.5 are presented in Fig. 10 (ref. 6). These interferograms were recorded at different angles of attack for the fast schedule used. It is clear from the

fringe pattern in Fig. 10 that the flow is fully attached at α = 12.03 deg, for shape 2. Attached flow is also seen for α = 15 deg, for shape–7.5, although some disturbance is noticeable in this figure near x/c $\approx$ 0.1. Results presented in ref. 3 show that the flow over the fixed, shape–8.5, airfoil generally behaves similarly to that seen in Fig. 10 with slight differences in the angle of attack of the events. It is noted here that on an NACA 0012 airfoil, dynamic stall onset occurs at α = 14 deg at M = 0.3. In contrast, on the DDLE airfoil, the flow was fully attached (not shown) even at α = 16 deg, highlighting one benefit of dynamic shape adaptation. Traces of trailing edge separation are present for α = 17 deg over the shape–7 airfoil, which become more pronounced for α = 18 deg and for α = 19 deg. A look at the leading edge image reveals the presence of a large number of fringes in the flow, indicating the continued development of strong leading edge suction, even when trailing edge separation has progressed up to x/c $\approx$ 0.1 on the upper surface. At α = 20 deg, the maximum number of fringes has decreased and hence, the peak suction pressure has dropped, but the leading edge flow remains attached. During the downstroke, the flow at α = 19 deg and α = 18 deg (not shown) appears similar to that seen on the upstroke at these angles, the only difference being that the maximum number of leading edge fringes is fewer on the downstroke. As the return to the original airfoil shape begins, light dynamic stall is induced at α = 16 deg, in much the same way as was seen for the fixed shape–8.5 airfoil (ref. 3). This is because the flow has to adjust to the more favorable conditions– in particular to the lower levels of vorticity flux associated with these lower angles of attack - to prevent build up of vorticity. Most interestingly, fully reattached flow develops at the high angle of attack of 15 deg on the downstroke for the shape–5 airfoil, and the suction peak becomes well established again. In contrast, at this angle of attack, light dynamic stall was present in the flow over the fixed shape–8.5 airfoil as reported in ref. 1, leading to the conclusion that the DDLE airfoil is better than a fixed shape–8.5 airfoil. Fig. 10 also shows that it is possible to manipulate the flow field in order to keep the leading edge flow attached throughout the oscillation cycle. Similar results were obtained for the slow schedule also.

The major difference between the NACA 0012 airfoil and the DDLE airfoil flow fields is the absence of the dynamic stall vortex in the latter. Thus, it is clear that the vorticity fields in the two cases are also different. The absence of the dynamic stall vortex leads to the deduction that the pitching moment variations over the DDLE airfoil tend to be milder, and the range of angles of attack over which the flow remains attached considerably larger when compared to the NACA 0012 airfoil. Dynamic shape adaptation has successfully altered the flow vorticity field, leading to changes in the airfoil stall behavior from leading edge type to the trailing edge type. If the time scale of airfoil oscillation and airfoil adaptation can be carefully matched to diffuse the excess vorticity on the downstroke, then it may even be possible to avoid the light dynamic stall condition encountered normally. This requires returning to the original shape very slowly. However, since the airfoil oscillation frequency is derived from a rotor flow condition, the airfoil adaptation rates are bounded. Hence, attempts to eliminate the light dynamic stall state may be impractical in real use.

3.G. Peak Suction Development

In Fig. 11 (ref. 7), the development of the airfoil peak suction pressure coefficient $C_{p_{min}}$ is compared for the NACA 0012, fixed shape–8.5, and the DDLE airfoil geometries at the two deformation rates used. Within experimental uncertainty, the peak suction values for the two deformation rates show nearly the same variation, even though the shape adaptation was initiated at different angles of attack. The NACA 0012 airfoil generates the highest value of $C_{p_{min}}(\approx -7.5)$, which indicates that the flow has become locally supersonic ($C_{p_{crit}} \approx -7.0$ at $M = 0.3$), however, no shocks are seen. In both the fixed shape airfoil case and the DDLE airfoil case, $C_{p_{min}}$ just reaches the critical value with the fixed shape–8.5 airfoil showing a slightly more gradual fall of peak suction pressure. On the upstroke, the values for the DDLE airfoil are slightly higher, suggesting that the suction lift over it tends to be marginally higher. Of greater interest is the 30% smaller size of the peak suction pressure loop for both the DDLE cases. This difference between the fixed shape–8.5 and DDLE airfoil cases in both the upstroke and downstroke peak suction
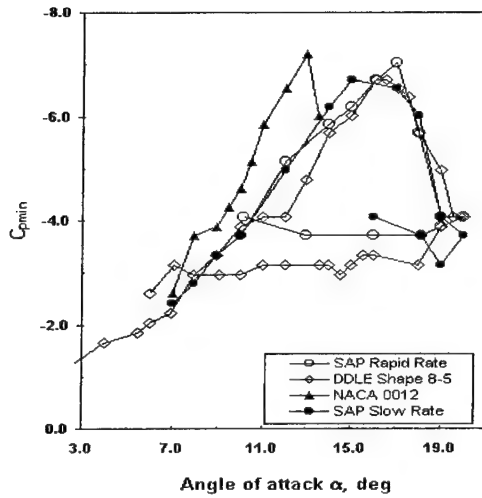
Fig. 11. Comparison of peak suction development over the SAP, shape 8.5 and NACA 0012 airfoils; M = 0.3 and k = 0.05.
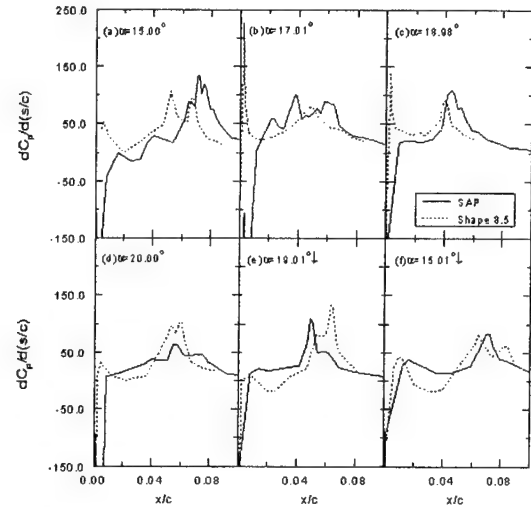

Fig. 12. Vorticity flux development over the shape 8.5 and SAP airfoils; M = 0.3 and k = 0.05.

pressures is due to the different extents of trailing edge separation present over the airfoils since there was no dynamic stall vortex in both flows. Because the flow reattaches at α = 15 deg for the DDLE cases as opposed to at $\alpha \approx$ 12 deg for the fixed shape–8.5 case, its loop is smaller. In contrast, for the NACA 0012 airfoil, the shedding of the large dynamic stall vortex causes the flow to separate completely. Complete reattachment does not occur until $\alpha \approx$ 8 deg on the downstroke (ref. 8). The large $\Delta\alpha$ between separation and reattachment results in a very large hysteresis loop in the moment coefficient as well. If shape adaptation were ideal and complete, a difference in the $C_{p_{min}}$ development between the upstroke and downstroke would not be present because the flow vorticity would be diffused through the boundary layer at a rate consistent with its production throughout the oscillation cycle. **This should indeed be the goal of shape adaptation**. In reality, one can only expect to minimize the hysteresis loop so that the airfoil can deliver a performance that is free from large-scale separation effects. The results presented here confirm that satisfactory shape adaptation was achieved for this experimental condition of M = 0.3 and k = 0.05.

26

It is noted here that the shape adaptation for the slow case was initiated at $\alpha \approx 3.8$ deg and for the rapid case at $\alpha \approx 8$ deg, these angles being determined from the attached flow envelope developed in Fig. 5. The primary factor that controls the shape change schedule is the attached flow envelope for each Mach number. **The requirement to satisfy, for potential success, is that any instantaneous shape reached should be within this envelope for the flow at any angle to remain attached**. The delay in pressure field development produced due the lag effects of unsteady flow provides some latitude in this regard.

It was also observed in these studies that initiating the deformation at inappropriate angles of attack induced premature dynamic stall. Thus, it is very important to determine the attached flow envelope in steady flow first, before proceeding with dynamic stall flow control. More details on this can be found in ref. 6.

3.H. Vorticity Flux Distributions

The vorticity fluxes calculated from the PDI derived pressure distributions (see ref. 3) for the fixed shape–8.5 and the DDLE airfoils are compared in Fig. 12. The large changes in the potential flow due to large real-time geometry modifications translate to a large effect on the pressure distribution, which should be seen in the vorticity flux also. At $\alpha = 15$ deg, the vorticity flux over the rapidly adapted DDLE airfoil is generally lower than that over the fixed shape–8.5 airfoil. The location of the peak vorticity flux value over the DDLE airfoil moves toward the trailing edge at $x/c \approx 0.08$ in Fig. 12a. No comparisons can be made with the distributions for the NACA 0012 airfoil since dynamic stall occurs at $\alpha = 14$ deg and the flow separates completely by $\alpha = 16$ deg. However, it was shown in Sec. E that the vorticity flux distributions over the fixed shape–8.5 airfoil were significantly superior to that over the NACA 0012 airfoil at the lower angles of attack, because of its lower maximum value and downstream location of the peaks.

Figure 12 establishes that on the upstroke, the DDLE airfoil flow is generally better than that of the fixed shape–8.5 airfoil. The peak vorticity flux for the DDLE airfoil moves

27

slightly upstream with increasing angle of attack (from x/c = 0.08 to x/c = 0.05, Fig. 12b-d), but it is lower than that for the shape-8.5 airfoil. The large peak of 225 seen for the fixed shape–8.5 airfoil close to the leading edge in Fig. 12b is not observed for the DDLE airfoil, even though its instantaneous shape of 7.5 attained dynamically is very close to the fixed shape–8.5. This can be attributed to the extreme sensitivity of the flow to the dynamic change of leading edge curvature. At α = 20 deg, Fig. 12d, the peak vorticity in the DDLE airfoil flow drops to about 50% of that seen in the fixed shape–8.5 airfoil flow, occurring at x/c = 0.05. In this, the peak vorticity occurs away from the leading edge and is significantly lower, when compared to the NACA 0012 airfoil prior to onset of dynamic stall. This explains why no dynamic stall vortex was observed in the deforming airfoil flow. On the downstroke at α = 19 deg, Fig. 12e, the DDLE airfoil flow vorticity level is somewhat higher and leads the fixed shape-8.5 airfoil, a trend that can be traced to the fact that the peak suction pressure is higher during the downstroke for the DDLE airfoil. In Fig. 12f, the values for the fixed shape–8.5 airfoil are compared at α = 15.5 deg with the DDLE airfoil at α = 15 deg. The higher vorticity flux levels suggest that a somewhat improved lift performance can be expected from the DDLE airfoil because of the increased circulation due to this vorticity.

3.I. Characteristics of the DDLE Airfoil Flow at M = 0.4, k = 0.05

The DDLE airfoil was adapted from shape-0 to shape-6 in this case based on the attached flow envelope shown in Fig. 6 (ref. 3). The actual deformation schedule used is shown in Fig. 13 (ref. 9). Figures 13 and 14 (ref. 9) show the flow development over the NACA 0012 and the DDLE airfoils, respectively. Shocks develop over the former by α = 10 deg (Fig. 14a) and shock-induced dynamic stall ensues by α = 10.5 deg, (Fig. 14b) with deep dynamic stall following at α = 12.5 deg as can be seen in Fig. 14c. The figures show that the whole process occurs over a very small angle of attack range. The flow remains fully stalled until $\alpha \approx$ 10 deg on the downstroke.

In contrast, the DDLE airfoil, whose shape is varied from shape-0 to shape-6 shows many different flow features. At α = 9 deg Fig. 15a, the flow over the leading edge is fully

28

attached. A small separation bubble is seen beyond x/c ≈ 0.08. The airfoil has been nearly deformed to shape-6 (which corresponds to a leading edge movement of only 0.018in) by this angle. As the airfoil pitches up, shocks develop near the leading edge region and by
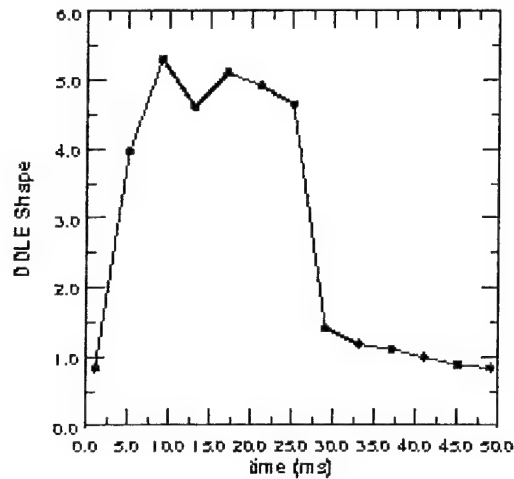

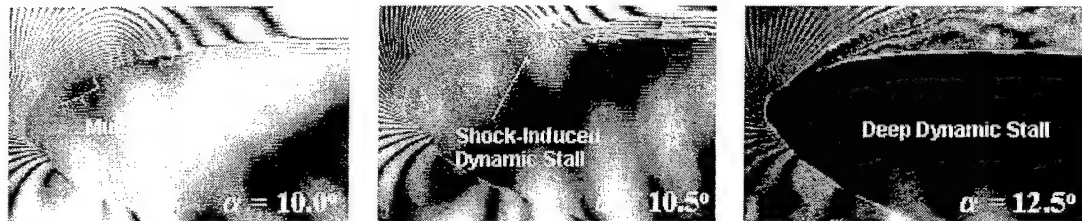Fig. 13. Typical DDLE airfoil shape-change profile, M = 0.4 and k = 0.05.

Fig. 14. PDI Images of flow over the NACA 0012 airfoil, M = 0.4
and k = 0.05; (a) α = 10.0 deg, (b) α = 10.5 deg and (c) α = 12.5 deg.

α = 13 deg, (Fig. 15b, shape-5.7) it appears that light dynamic stall is initiated on the upstroke, downstream from the foot of the shock. During this stage, the vorticity downstream of the shock is shed. This process continues as the airfoil pitches-up and eventually stops by α = 19 deg, Fig. 15c, shape-5.6. The leading edge flow is fully attached, but with fewer fringes, implying a decreased peak suction value. The technique has been successful in delaying unsteady stall by about 7 degrees when compared to the

29

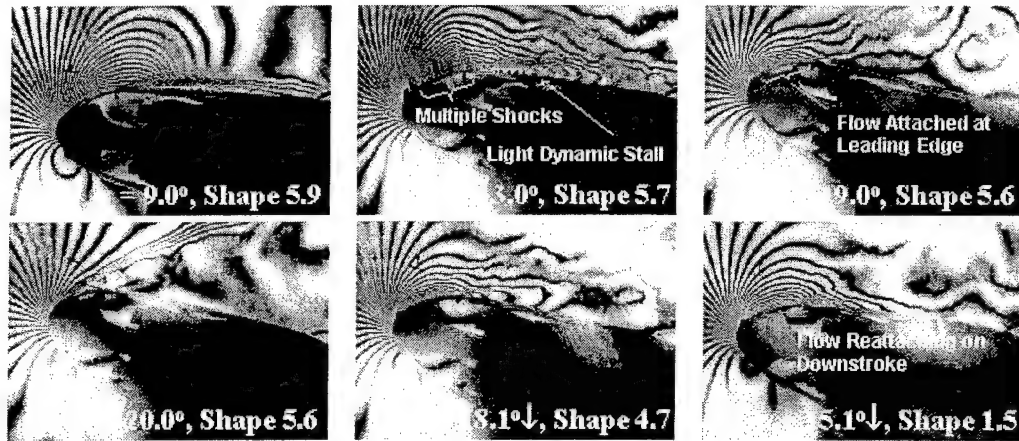fixed NACA 0012 airfoil. Further increase in α results in a brief period of separation

Fig. 15. PDI Images of flow over the DDLE airfoil, M = 0.4 and k = 0.05; (a) α = 9.0 deg, shape 5.9; (b) α = 13.0 deg, shape 5.7; (c) α = 19.0 deg, shape 5.6; (d) α = 20.0 deg, shape 5.6; (e) α = 18.1 deg $\downarrow$, shape 4.7; and (f) α = 15.1 deg

from the leading edge as shown in Fig. 15d, α = 20 deg, shape-5.6. However, the leading edge flow quickly reattaches, Fig. 15e, α = 18 deg, shape-4.7 on the downstroke. By α = 16 deg on the downstroke and shape-1.5, (Fig. 15f) while re-forming the NACA 0012 airfoil, the flow has nearly fully reattached. Thus, the attached flow regime for the DDLE airfoil extends over a much larger angle of attack range than for the NACA 0012 airfoil. Most importantly, there is no organized dynamic stall vortex as was seen for the NACA 0012 airfoil, and the airfoil produces suction lift for most of the oscillation cycle when the leading edge flow remains attached. This behavior is almost similar to that seen for the fixed shape-6 airfoil (Ref. 3) whose leading edge flow was attached throughout the cycle. Since the airfoil has to change its shape for acceptable performance on the advancing side, a slight leading edge separation without the dynamic stall vortex may be a modest price to pay. Furthermore, the decreased drag possibility of this design on the advancing side makes it preferred method for controlling the rotor dynamic stall flow.

In comparison, the shape adaptive airfoil flow develops an even higher peak suction pressure of -4.9 (ref. 9), Fig. 16, a value attained at α = 16 deg. It is also interesting to see

that the $C_{p_{min}}$ plot appears like the natural extension of the NACA 0012 airfoil as its shape is adapted. The loss of the suction peak occurs at a rate comparable to that observed for the slatted airfoil, but as the flow visualization pictures discussed earlier revealed, the recovery is also quicker and by $\alpha = 16$ deg on the downstroke, the value is fairly high at ≈ -3.4. Despite the small amount of flow separation seen, it can be concluded from Fig. 16 that acceptable shape adaptation can be achieved for this flow condition.
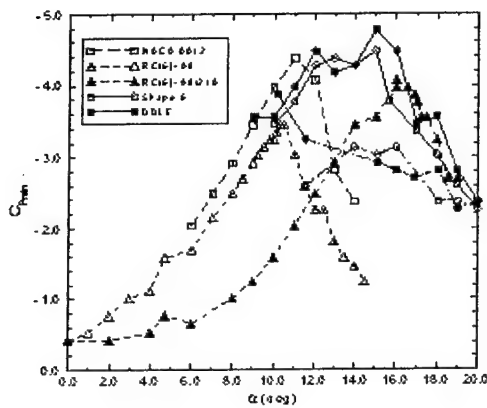

Fig. 16. Development of suction peak on various airfoil configuration for $M = 0.4$ and $k = 0.05$.
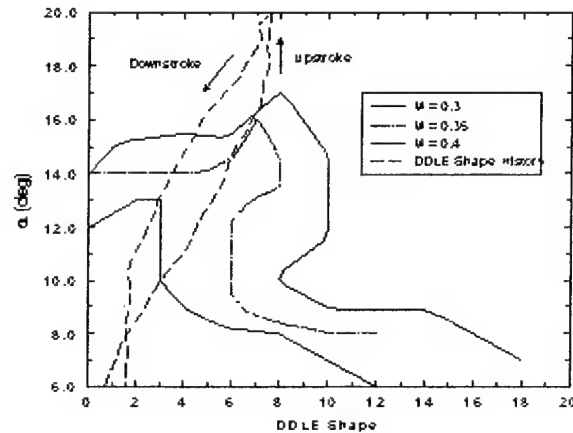

Fig. 17. Attached flow envelopes for the DDLE airfoil for $M = 0.3$, 0.35 and 0.45.

$C_{p_{min}}$ values that were calculated from the maximum number of fringes seen in Fig. 14 and 15 show that the DDLE airfoil generally develops about 15-20% higher peak suction values, which is clearly desirable. Thus, shape adaptation, which is necessary to satisfy the geometry requirements on the advancing side is also beneficial. The reason for the increased suction peak pressures appears to be the favorable interaction between the two unsteady time scales present in the flow – namely, the airfoil reduced frequency and the shape adaptation rate – both of which contribute to the unsteady term in the vorticity flux equation. Together, these seem to induce a pronounced effect on the vorticity flux manipulation.

3.J. Do Compressibility Effects on Attached Flow Envelope Negate Flow Control Efforts?

The noticeable reduction of the size of the attached flow envelope for M = 0.4 compared to M = 0.3 poses the question whether the concept can be indeed be useful in practical applications, where a rotor blade starts pitching up from a high Mach number of 0.4-0.45. Because compressibility promotes dynamic stall, its onset occurs at a very low angle of attack (< 8-10 deg) at M = 0.45. Thus, for this flow to be controlled, the shape adaptation should be initiated from a rotor azimuthal position where the Mach number is still high at a low angle of attack. As the rotor retreats, its Mach number decreases and thus, a larger range of airfoil shapes become available for flow control to progress because of the expanded attached flow envelope at the lower Mach numbers, as seen in Fig. 17. Thus flow control can continue well into the retreating side. A possible shape change schedule is shown in Fig. 17. Since there is a lag in the development of the unsteady flow development, it may be even possible to exceed the boundaries slightly from that shown. This leads to the conclusion that the use of the DDLE concept provides significant opportunity at achieving dynamic stall control.

3.K. Surface Hot Film Gage Studies

In an attempt to understand the events of dynamic stall, the surface shear stress was qualitatively studied using a dense array of hot film gages. These were mounted on a solid 6-inch chord NACA 0012 airfoil at a spacing of 40 gages/in from $x/c = 0.1$ on the lower surface to $x/c = 0.25$ on the upper surface. Further downstream, a 4-gage set was distributed at the same pitch in x/c increments of 0.05. This distribution resulted in a total of 120 gages on the airfoil upper surface. For ease of reference, the gages are referred to by their numbers, with gage no. 1 at $x/c = 0.95$ and gage no. 120 at the leading edge. Gage number 60 was at $x/c = 0.25$ due to the high pitch used. These were operated using TSI hot wire bridges Model 1750/1755 provided by the US Air Force Academy. Data from 16 sensors was acquired at a time at rates of up to 40KHz per channel.

Since no calibration method exists for quantitative estimation of the skin friction, only a qualitative analysis of the data was conducted. In the various plots presented here, the

ensemble averaged mean value over many cycles has been subtracted and only, the deviations from this are plotted.

The results provide the first recordings of the rapid upstream movement of the transition point in unsteady compressible flow at these conditions from x/c ≈ 0.6 at α = 1 deg to x/c ≈ 0.02 at α = 7-8 deg. A typical case is shown in Fig. 18 for M = 0.3, k = 0.05. A surface map of this is presented in Fig. 19. The heat flux over the initially laminar flow steadily
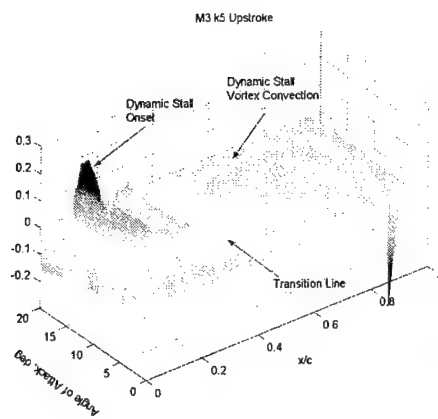

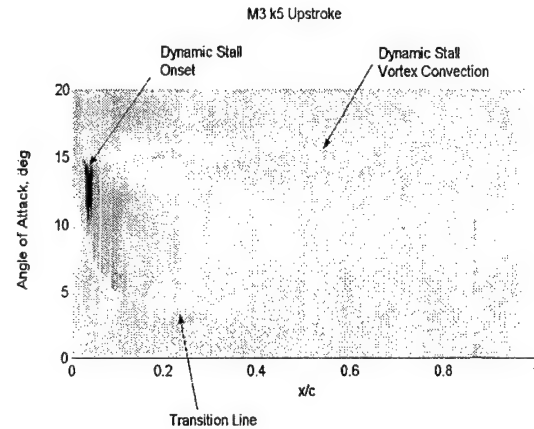Fig. 18. Heat flux gage outputs on the NACA 0012 airfoil upper surface, M = 0.3, k = 0.05 and upstroke.

Fig. 19. Heat flux gage outputs on the NACA 0012 airfoil upper surface, M = 0.3 and k = 0.05, upstroke, Surface map showing the rapid movement of transition point.

falls as the boundary layer gradually thickens due to increasing angle of attack. Suddenly, transition occurs, which is seen as a rise in heat flux (color change from shades of blue to shades of red) for α ≈ 1 deg at x/c = 0.562 and moves to x/c = 0.08-0.09 α ≈ 4.8 deg.

However, upstream of this, another dominant flow feature develops, seen in Fig. 20. For 0.05 < x/c < 0.1 the heat flux shows a sudden drop (the blue region) at about the same angle of attack of ≈ 6 deg, which is related to local laminar flow separation. The separated shear layer reattaches to form the laminar separation bubble. As the airfoil is pitched up to a higher angle, the upstream end of the laminar bubble moves towards the

leading edge. The downstream end of the bubble does not appear to move since the flow downstream of it has already become fully turbulent.

It is interesting to see significant variations in the heat flux are present within the bubble region (see indicated region in Fig. 20). Over the sensors near the leading edge the heat flux keeps falling, indicating that the flow reversal is still ongoing at angles of attack
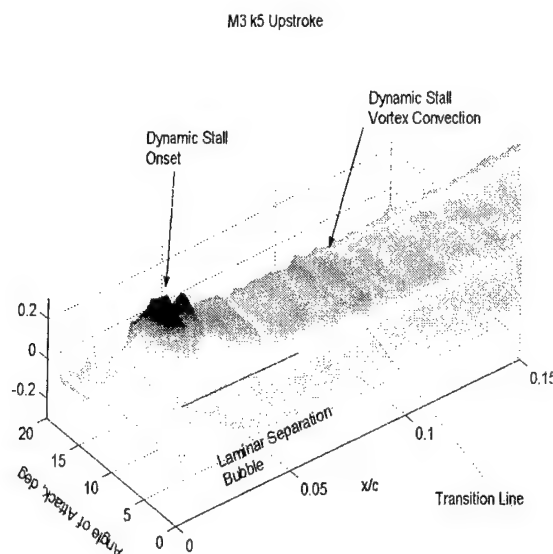

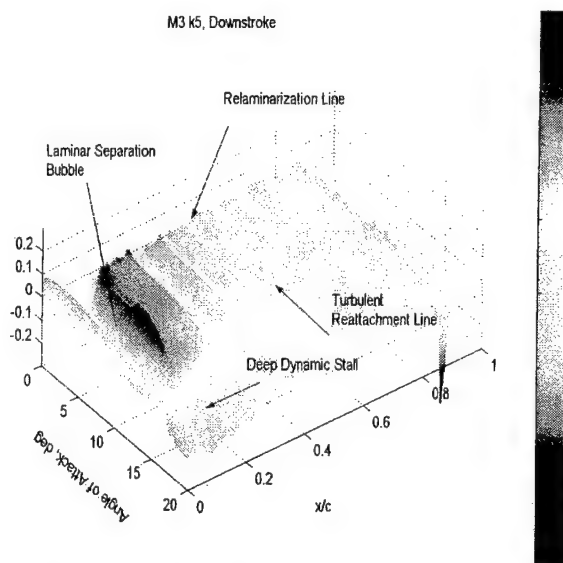Fig. 20. Heat flux gage outputs on the NACA 0012 airfoil upper surface in the bubble region, M = 0.3 and k = 0.05

Fig. 21. Heat flux gage outputs on the NACA 0012 airfoil upper surface showing reattachment, M = 0.3, k = 0.05 and downstroke.

slightly higher than the bubble formation angle. Then, there is a rapid rise in the heat flux at the leading end of the bubble and a more gradual rise at its trailing end. It is believed that part of this is due to the strong recirculation that is locally present. However, there is an abrupt increase near the front end of the bubble, by an angle of attack of about 14.5-15deg, which can be attributed to the bubble break-down. Out of this process arises the dynamic stall vortex. Prior to the formation of the vortex, it is believed that there is violent activity within the bubble. The turbulence associated with this enhances the heat transfer, and the near identical angle of attack at which this rise is seen across several sensors in Fig. 20 leads to the conclusion that it is an abrupt process and occurs as the

34

bubble bursts. PDI pictures obtained earlier in this research also support this conclusion qualitatively and with good correlation in the angles of attack. Heat flux traces at other locations indicate a gradual progression of this peak to a slightly higher angle as the vortex convects over the upper surface as shown in Fig. 18. After the vortex passes, there is a sudden drop in the heat flux since there is virtually no flow behind it, a result once again supported by both schlieren and PDI pictures obtained in the facility. The shear layer is bounded to the leading edge and only encompasses the vortex.
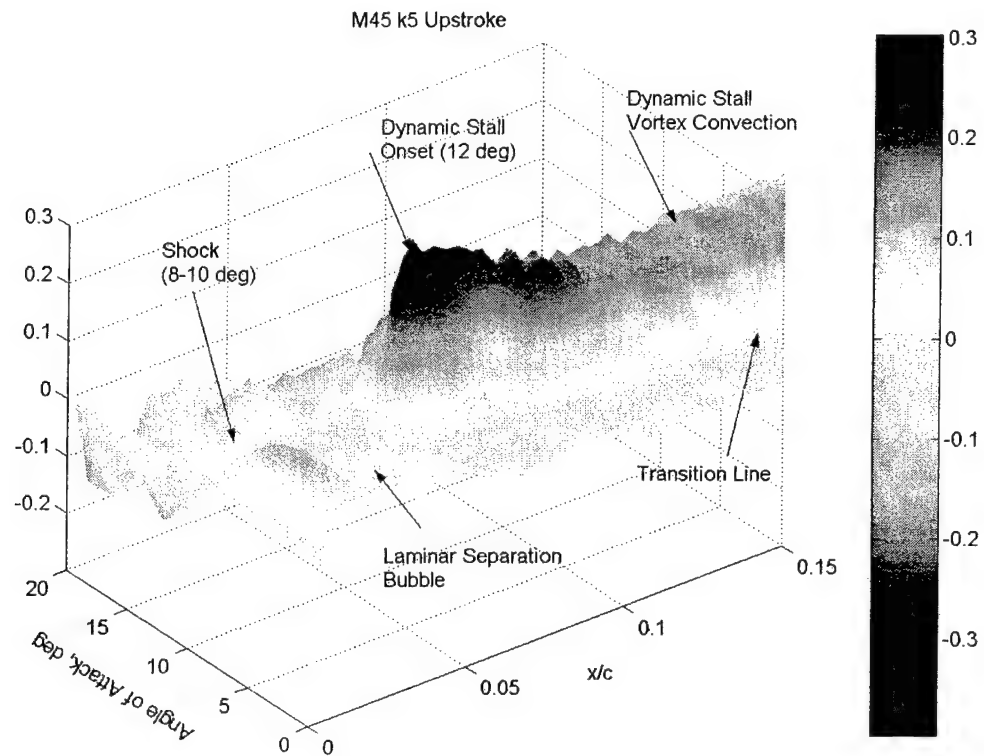
Fig. 22. Heat flux gage outputs on the NACA 0012 airfoil upper surface showing shocks and shock-induced dynamic stall onset, M = 0.45 and k = 0.05.

The low heat flux remains for much of the deep stall phase until the airfoil is at around 12 deg on the downstroke when the flow begins to reattach, Fig. 21. This process starts from the leading edge and proceeds in a systematic way. Eventually, the flow also relaminarizes and at very low angles of attack (< 1 deg) the flow is laminar up to about x/c = 0.6. The low signal levels in the region further downstream make it difficult to

discern the progress of the relaminarization. These details provide a clear documentation of the large changes in the transition and the surface shear stress that occur in this complex flow, a fact that needs to be included in the CFD modeling of the flow, that has hitherto not been done. Considerably better agreement with experimental data can be obtained if the appropriate physics such as described above is included in the models.

At M = 0.45, k = 0.05, the presence of shocks seen in the PDI pictures was also observed here, Fig. 21. Since the static temperature rises across a shock wave, the heat transfer from a heat flux gage at this location drops. Similarly, across an expansion wave, the heat transfer rises. The boundary layer near the leading edge where the shock forms is very thin, ($\approx$ 100 µm) and thus, the imprint of the shock can be picked up in the surface heat flux traces. Interpretation of this requires some prior knowledge of the flow, since only a rise or fall of heat transfer is measured. In this case, the PDI images from earlier experiments provided ample proof of the presence of multiple shocks and thus, one can infer the same in the heat flux gage experiments knowing the position of the sensors.

As angle of attack increases, more shocks form on the shear layer enveloping the bubble that forms for this condition, even before the shocks forms. Ultimately it appears that, the shear layer separates due to the pressure gradients imposed by the shocks. During this event, once again, there is violent activity in the bubble and dynamic stall originates from the separation. Its location is near the downstream end of the bubble unlike at M = 0.3, where it was from its upstream end. This type of separation is different from the pure bubble bursting induced event discussed for M = 0.3.

Due to the higher Reynolds number at M = 0.45, the transition point moves further upstream compared to the M = 0.3, k = 0.05 condition. The movement of transition point and the events of the shock and bubble interacting make this flow even more complex than discussed above and once again, need to be properly modeled for a better CFD analysis.

4. CONCLUSIONS

This study had two main foci: one was the establishment of the fluid mechanics of compressible dynamic stall control and the other was the study of the fluid mechanics processes of compressible dynamic stall.

For the first one, a dynamically deforming leading edge airfoil was tested in the CDSF. The major contribution was establishing the fact that compressible dynamic stall can indeed be controlled under helicopter retreating blade flow conditions. The establishment of the attached flow envelope was key in identifying the airfoil leading edge shapes that were needed during the process. The study also established that within this envelope, the dynamic stall vorticity could be produced and diffused at rates that maintained its peak level below the critical level for coalescence. This led to successful control of compressible dynamic stall both at $M = 0.3$ and 0.4 at a reduced frequency of 0.05. Another important result was that improper shape adaptation could promote dynamic stall onset, even prematurely. Hence, it is imperative that the leading edge deformation schedule be consistent with the vorticity balance requirements. In general slow rates of adaptation were found to be better at achieving success. Since the time scale of adaptation is not an independent quantity, but in fact is dependent upon the airfoil reduced frequency, this result becomes important both in terms of practical utility and in the fluid mechanics terms of vorticity management. The airfoil geometry was such that the large leading edge curvature required for flow control could be produced with a very small chordwise movement. In this study, less than 0.4% of chord, a maximum linear chord length change of 0.025in was used. This small change appears within the realm of present day smart materials and actuators, offering the hope that the technique could become practical.

The heat flux gage studies documented the rapid movement of the transition onset point as a function of angle of attack. They also showed that there is violent activity in the bubble or under a separated shear layer at a higher Mach number of 0.45 prior to dynamic

stall onset, which lends support to the idea that the different dynamic stall onset processes - identified by the author in previous ARO sponsored projects - are singular events.

5. LIST OF PUBLICATIONS AND TECHNICAL REPORTS

1. M.S.Chandrasekhara, M.C. Wilder and L.W.Carr, "Compressible Dynamic Stall Control Using Dynamic Shape Adaptation", (AIAA Paper 99-0650), *AIAA Journal*, Vol. 39, No. 10, pp. 2021-2024.

2. M.S.Chandrasekhara, M.C. Wilder and L.W.Carr, "Compressible Dynamic Stall Control: Comparison of Two Approaches", (Invited AIAA Paper 99-3122), *Journal of Aircraft*, Vol. 38, No. 3, pp. 448-453, May-Jun. 2001.

3. M.S.Chandrasekhara, M.C.Wilder, and L.W.Carr, "The Control of Compressible Dynamic Stall Using Adaptive Airfoils", *IUTAM Symposium on Mechanics of Passive and Active Flow Control"*, Kluwer Academic Publishers, FMIA Vol. 53, pp. 75-80, Aug. 1999.

4. M.S.Chandrasekhara, M.C.Wilder, and L.W.Carr, "Unsteady Stall Control Using Dynamically Deforming Airfoils", (AIAA Paper 97-2236), *AIAA Journal,* Vol. 36, No. 10, Oct. 1998, pp. 1792-1800.

5. M.S.Chandrasekhara, M.C.Wilder, and L.W.Carr, "On the Competing Mechanisms of Compressible Dynamic Stall", (AIAA Paper 96-1953), *AIAA Journal,* Vol. 36, No. 3, March 1998, pp. 387-393.

6. M.S.Chandrasekhara, L.W.Carr, M.C.Wilder, C.Hiel, C.D.Sticht, and G.N.Paulson, "Design and Development of a Dynamically Deforming Leading Edge Airfoil for Unsteady Flow Control", *ICIASF'97 RECORD*, IEEE Publication No. 97CH36121, pp. 132-140.

7. M.S.Chandrasekhara, L.W.Carr, and M.C.Wilder, "Development of High Speed Imaging and Analysis Techniques for Compressible Dynamic Stall", *AGARD –CP – 522*, May 1998, pp. 21.1-21.12.

8. M.Sahin, L.N.Sankar, M.S.Chandrasekhara and C.Tung, "Dynamic Stall Alleviation Using a Deformable Leading Edge Concept – A Numerical Study", AIAA Paper 00-0520, Reno, NV, Jan. 2000.

9. M.S.Chandrasekhara, "Review of Compressible Dynamic Stall and Its Control", *Invited Paper*, Proc. of the 8th Asian Congress of Fluid Mechanics, International Academic Publishers, Shenzhen, China, pp. 47-50.

10. W.Geissler, L.W.Carr, M.S.Chandrasekhara, M.C.Wilder and H.Sobieczky, "Compressible Dynamic Stall Calculations Incorporating Transition Modeling for Variable Geometry Airfoils", AIAA Paper 98-0705 , Reno, NV, Jan. 1998.

11. M.S.Chandrasekhara, M.C.Wilder, and L.W.Carr, "Fluid Mechanics of Wing Adaptation for Separation Control", 7th Asian Congress of Fluid Mechanics, Madras, India, Dec. 8-12, 1997.

12. W.Geissler, M.S.Chandrasekhara, M.F.Platzer and L.W.Carr, "The Effect of Transition Modeling on the Prediction of Deep Dynamic Stall", 7th Asian Congress of Fluid Mechanics, Madras, India, Dec. 8-12, 1997.

13. M.S.Chandrasekhara, M.C.Wilder and L.W.Carr, "Unsteady Stall Control Using Dynamically Deforming Airfoils", AIAA Paper 97-2236, Atlanta, GA, Jun. 1997.

6. LIST OF ALL PARTICIPATING PERSONNEL

1. Professor M.S. Chandrasekhara, NPS, Monterey, CA
2. Dr. L.W. Carr, Cooperative Participant, US Army AFDD/AMCOM
3. Dr. M.C. Wilder, Eloret Institute, San Jose, CA

7. REPORT OF INVENTIONS

None.

8. BIBLIOGRAPHY

1. M.S.Chandrasekhara, L.W.Carr, M.C.Wilder, C.Hiel, C.D.Sticht, and G.N.Paulson, "Design and Development of a Dynamically Deforming Leading Edge Airfoil for Unsteady Flow Control", *ICIASF'97 RECORD*, IEEE Publication No. 97CH36121, pp. 132-140.

2. N.J. Brock, M.S.Chandrasekhara, L.W.Carr, "A Real Time Interferometry System for Unsteady Flow Measurements", ICIASF Publication No. 91CH3028-8, pp. 423-430.

3. M.S.Chandrasekhara, M.C.Wilder, and L.W.Carr, "Unsteady Stall Control Using Dynamically Deforming Airfoils", (AIAA Paper 97-2236), *AIAA Journal,* Vol. 36, No. 10, Oct. 1998, pp. 1792-1800.

4. L.W.Carr and M.S.Chandrasekhara, "A Review of Compressibility Effects on Dynamic Stall of Airfoils", AIAA Paper 95-0779, **Invited Paper**, Reno, NV, Jan. 1995.

5. W.C.Reynolds and L.W.Carr, "Review of Unsteady, Driven, Separated Flows", *AIAA Paper 85-0527*, Mar. 1985.

6. M.S.Chandrasekhara, M.C.Wilder, and L.W.Carr, "Compressible Dynamic Stall Control Using a Shape Adaptive Airfoil", AIAA Paper 99-0650 Reno, NV, Jan. 1999

7. M.S.Chandrasekhara, M.C. Wilder and L.W.Carr, "Compressible Dynamic Stall Control Using Dynamic Shape Adaptation", (AIAA Paper 99-0650), *AIAA Journal*, Vol. 39, No. 10, pp. 2021-2024.

8. S.Ahmed and M.S.Chandrasekhara, "Reattachment Studies of an Oscillating Airfoil Dynamic Stall Flow Field", *AIAA Paper No.* 91-3225, Sep. 1991.

9. M.S.Chandrasekhara, M.C. Wilder and L.W.Carr, "Compressible Dynamic Stall Control: Comparison of Two Approaches", (Invited AIAA Paper 99-3122), *Journal of Aircraft*, Vol. 38, No. 3, pp. 448-453, May-Jun. 2001.